Hindawi
Advances in Meteorology
Volume 2022, Article ID 6953306, 13 pages
https://doi.org/10.1155/2022/6953306

Research Article

Impact of Hydroclimate Change on the Management for the Multipurpose Reservoir: A Case Study in Meishan (China)

Yang Liu [1] **and Buwei Wang** [2]

[1]*Key Laboratory of Land Surface Pattern and Simulation, Institute of Geographic Sciences and Natural Resources Research, Chinese Academy of Sciences, Beijing 100101, China*
[2]*China Electric Power Research Institute Co.Ltd, Beijing 100192, China*

Correspondence should be addressed to Yang Liu; liu_yang@igsnrr.ac.cn

Received 23 November 2021; Revised 10 March 2022; Accepted 15 March 2022; Published 30 March 2022

Academic Editor: Upaka Rathnayake

China holds the largest amount of reservoirs in the world, while more than 80% of them were constructed 50–70 years ago and are approaching a critical stage of their designed lifetime. Before deciding the future of a reservoir, it is essential to find out whether it could still satisfy its original purpose in the context of hydroclimate change under global warming. Here, we present a case study of the Meishan reservoir in east-central China, which was primarily built for irrigation and flood control in the 1950s. We evaluate the impacts of rainfall change on the hedging and releasing rules over the historical period (1969–2008) by instrumental data and future period (2061–2100) based on simulations in a regional rivalry-mitigated scenario from the Coupled Model Intercomparison Project Phase 6. The main conclusions are as follows: (1) the annual total rainfall has a remarkable increasing trend from 2015 to 2100 and the annual precipitation variability exceeds the envelope range during the past 50-year period. The increased precipitation amount mainly occurs in spring (March to May). (2) The optimal regulation cycle is from September to August and from July to June for both historical and future periods. The limiting level during the nonflooded season is lower than the operating water level for more than five months in the historical period, which limits the ability of reservoir regulation and utilization of water resources. However, the water supply is no longer affected by flood control in 2061–2100 because of the redistribution of annual precipitation. (3) The projected irrigation and residential water demands of the Meishan reservoir are stable; thus, the improvement of the total economic benefit will mainly depend on power generation. This case provides a practical guide for many reservoirs serving water supply for small cities in eastern China, where the size of the population and cultivated land area is stagnant and the climate is getting wetter.

1. Introduction

Reservoir and dam system stores additional water in the rainy season and releases it in drier months, playing a fundamental role in achieving sustainable uses of the water resource. In practice, the storage or empty space to be maintained in a reservoir during different times of the year is determined by the rule curve, which is predefined in the design stage based on long-term (30 years or more) water inflow and demand statistics. Generally, the rule curve is fixed during the lifespan (~ a hundred years) of reservoirs [1, 2]. Almost 50% of hydropower reservoirs worldwide were originally commissioned more than 40 years ago [3], meaning that their rule curves are calculated from climate data in the mid-twentieth century or even earlier times. However, many observed changes in the climate system during the past decades are unprecedented over centuries, including precipitation and temperature-induced evaporation [4], which have already affected the regional runoff [5]. For the rest of the twenty-first century, the precipitation is projected to increase over high latitudes in parts of the monsoon regions and in wet regions over the tropics, but decrease in dry regions including large parts of the subtropics under 1.5°C and 2°C global warming scenarios. The changing patterns of precipitation minus evaporation and runoff are similar to precipitation [4]. Consequently, the

predefined reservoir rule curve in the mid-twentieth century may not remain as effective operation guidance in current and future situations. Moreover, aged reservoirs are about to reach the designed service life [3]. Maintaining or demolishing these reservoirs in the future requires an overall assessment of the energy-related benefits and ecological environment impacts, in which the most important issue is whether the reservoirs could still satisfy their original purpose in the context of hydroclimate change under global warming.

Studies on evaluating the impacts of climate change on reservoir management are carried out all over the world, for example, in northwest America [6], southeast Canada [7], eastern India [8], and northeast Thailand [9, 10]. Among countries owing dam-reservoir systems, China counts more than 40% of the total in the world [11]. Thus, a large number of cases are conducted in China, located in the Yangtze River basin [12–15], Xin'an River basin [16], Hai River basin [17], Yuan River basin [18], and Zhu River basin [19]. Some studies [12–14, 16–19] quantify the rainfall or streamflow change in the reservoir watershed and project the water budget in the future based on multiple theoretical models, but few of them provide the updated rule curves that could be directly used to guide the gate opening schedule of a dam. Others [6–10, 15] develop advanced optimization techniques to calculate rule curves but their future projections are extracted from a single climate model or based on previous-generation scenarios applied in the Coupled Model Intercomparison Project (CMIP) Phases 3 and 5. Now, the outputs of CMIP6 use a set of new plausible scenarios [4] and the multimodel ensemble is proved to be more reliable than a single model [20], which provides us more possible future pathways to assess the alteration of the rule curve under the climate change.

Over 80% of reservoirs in China were constructed between the 1950s and 1970s, most of which are not operated reliably and effectively now [21]. So far, however, the research in China mainly focuses on the electricity generation change of large or recently constructed hydropower reservoirs [12–14, 16, 18] and mega reservoirs serving the urban agglomerations [15, 17, 19]. There has been a little quantitative analysis of the rule curve change for the aged reservoirs. Here, we pay particular attention to the Meishan dam and reservoir system built during 1956–1958. It is located in Anhui Province (east-central China), where the province mean temperature and precipitation are projected to increase 2.3°C (with reference to 1850–1900) and 4.0% (with reference to 1985–2005) under 2°C global warming scenario [22]. Moreover, annual runoff changes in Anhui are basically consistent with precipitation, but the increased rates are different among seasons, that is, higher in spring and winter than in summer and autumn [23]. Thus, there is an urgent need to update the original regulating rules of Meishan reservoir developed 65 years ago. In this study, we use instrumental data for the past decades and the latest CMIP6 scenario simulations till 2100 to evaluate the potential impacts of climate change on the hedging and releasing strategies. A description of the study area, climate datasets, and statistical methods is given in Section 2. Regulating rule curves for historical and future periods are presented in Section 3. A summary of the main conclusions and the practical implications of the study case is discussed in Section 4.

2. Materials and Methods

2.1. Study Area. Meishan reservoir and dam project spans the Shi River in Anhui Province, eastern China (Figure 1(a)). Shi River is born in the Ta-pieh Mountains and joins the Huai River from the south side between Guan River and the west branch of Pi River (Figure 1(b)). The length of Shi River is 216 km and the catchment area is 6880 km^2. There are 11 branches upstream of the dam site, which is 130 km away from the confluence of the rivers Shi and Huai. The upstream watershed controlled by the dam is calculated from the hole-filled Shuttle Radar Topography Mission (SRTM) 90 m digital elevation data [24] by using a Matlab TopoToolbox [25]. The watershed area is 1970 km^2, which is mainly covered by forest and cropland (Figure 1(c)). The subtropical humid monsoon climate dominates the catchment area, where the annual mean temperature, precipitation, evaporation, and aridity are 15.5°C, 1381.5 mm, 1173.6 mm, and 0.8, respectively [26]. Meishan reservoir is a multipurpose facility and its main characteristics [27–29] are summarized in Table 1. The primary purposes are flood control and irrigation. The flood level is designed to accommodate an estimated 100-year recurrence interval event and it will provide the irrigation water needed for the agricultural sector to 25.5×10^2 km^2 farmland in five downstream counties (Figure 1(b)), that is, Jinzhai, Huoqiu, Liuan, Gushi, and Shangcheng [30]. Moreover, it releases the ecological flow to maintain the stability of the downstream ecosystem (e.g., biological protection, sediment deposition, and pollution control). However, hydropower generation is not mandatory and the turbines only work during irrigation season. The original capacity of the Meishan hydropower station was 40 MW, and it was increased to 52 MW after a retrofit project in 2012 [28].

2.2. Hydroclimate Observation and the Model for Predicting Inflow. The monthly inflow data at the dam site from 1969 to 2008 (Figure 2(a)) are provided by the Meishan hydrologic station, which could be used to directly calculate the water supply in the historical period. However, the water inflow is not an output variable of the CMIP6 models and we need to derive water inflow from other variables to calculate the water supply in the future period. Prior studies demonstrated that precipitation is the dominant factor of runoff in the upper-middle reaches of Huai River and its branches, while evaporation makes a minor contribution [31, 32]. Therefore, we test their relationships with water inflow. The rainfall data (1961–2014) are from a grid precipitation product [33] with a spatial resolution of 0.5°, and we use the data in the grid centered on 115.75°E, 31.75°N (Figure 2(b)) since it overlaps most of the reservoir area. The evaporation data are from the dataset of daily climate data from Chinese surface stations [34], and records of the nearest station

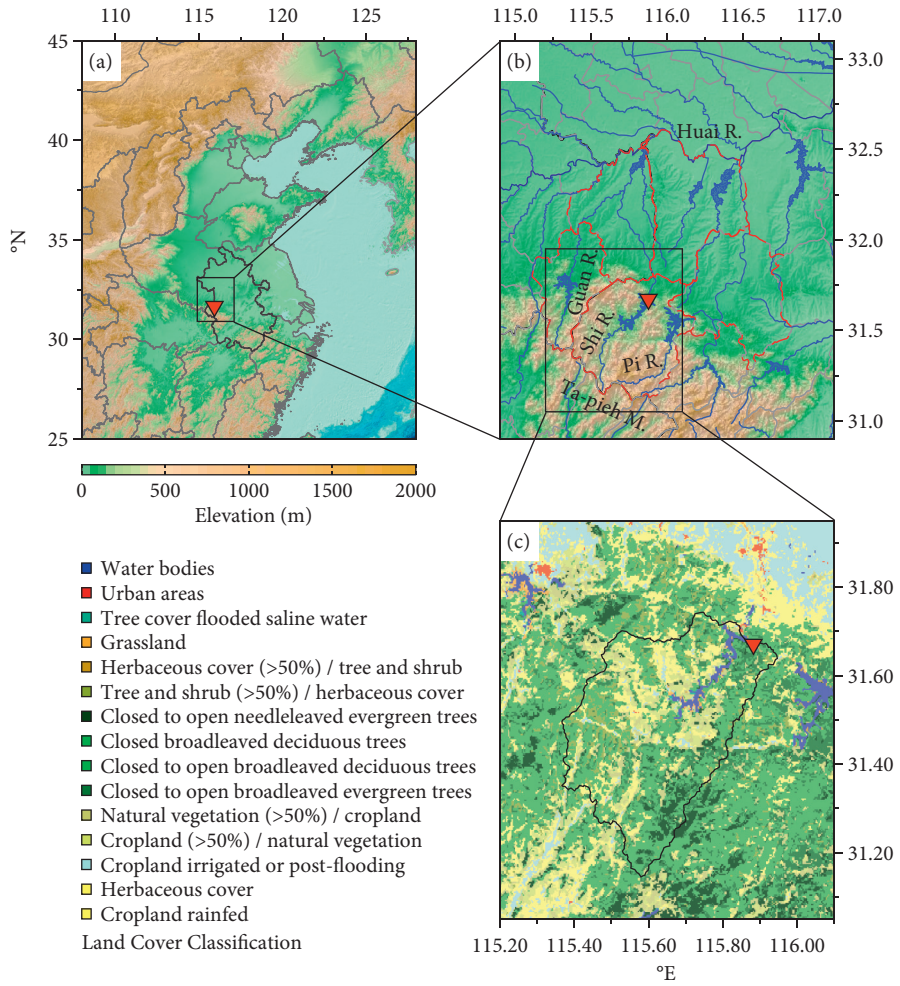

Figure 1: Basic geographic information of Meishan reservoir. (a) The location of Anhui Province (bold black line) in East Asia and the topography. (b) The location of the dam in Shi River and five counties (red dash line) irrigated by the reservoir. (c) The upstream catchment area of the dam and the land cover types in it. The red triangle indicates the dam position.

Table 1: Characteristics of the Meishan reservoir project [27–29].

Name	Value
Type of dam	Concrete multiple-arch dam
Controlled catchment area by the dam	1970 km^2
Total storage volume	22.63×10^8 m^3
Flood regulation capacity	10.65×10^8 m^3
Regulating storage	9.57×10^8 m^3
Dead storage	4.02×10^8 m^3
Annual mean inflow	14.05×10^8 m^3
Elevation of dam crest	140.17 m a.s.l.
Minimum operating elevation	107.07 m a.s.l.
Normal pool level	128.0 m a.s.l.
Dead water level	107.07 m a.s.l.
Design flood level	137.69 m a.s.l.
Check flood level	139.93 m a.s.l.
Limiting level during flood season	125.27 m a.s.l.
Limiting level during the nonflood season	126.0 m a.s.l.
Maximum dam height	88.24 m
Width crest	1.8 m
Top length of the dam	443.5 m

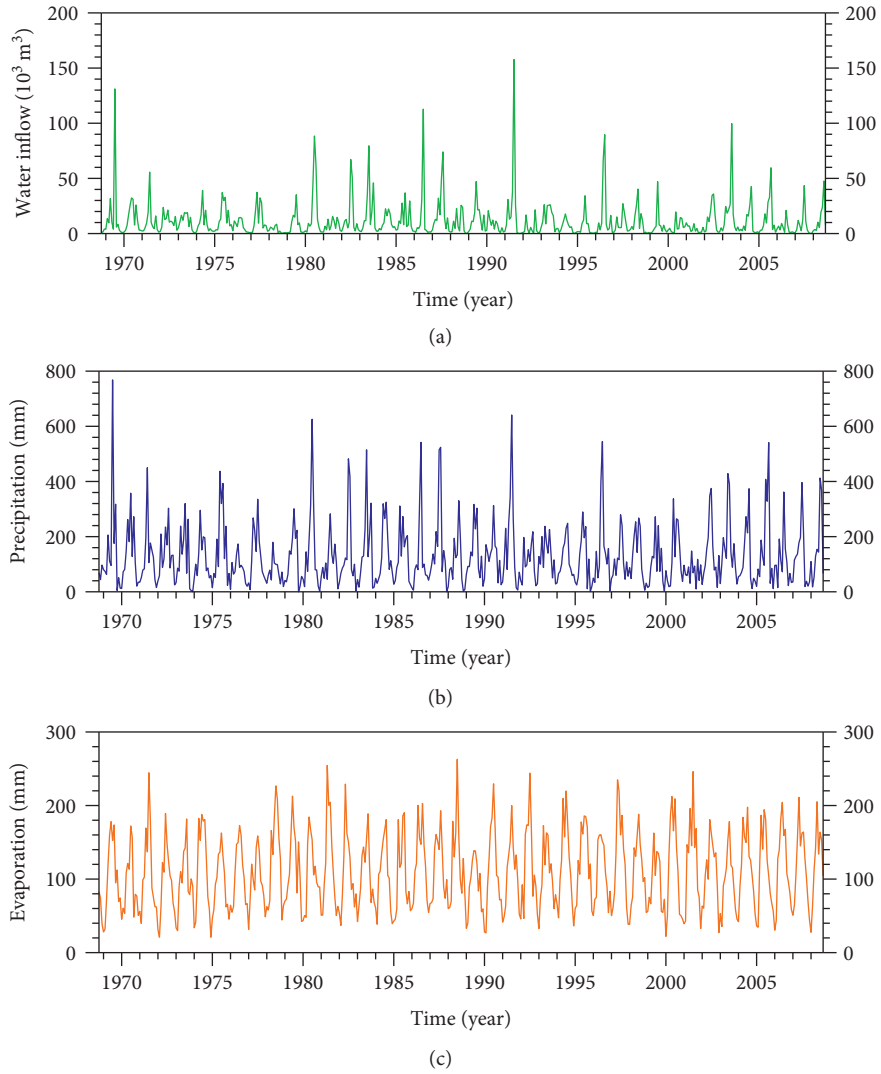

Figure 2: Monthly (a) water inflow, (b) precipitation, and (c) evaporation at Meishan reservoir.

(Jinzhai, 115.88°E, 31.68°N) are used to represent evaporation in the drainage basin (Figure 2(c)). Several regression models are calculated using different combinations of predictors and validated by the leave-one-out procedure (Table 2), and the result shows that the 2nd degree polynomial fitting by precipitation has the highest predicted variance of 85.99%. This nonlinear relationship is also observed in other reaches of the Huai River as that rains could induce more surface runoff after soil saturation [35]. However, introducing the evaporation parameter would reduce the model skill, such that only precipitation is used to predict future inflow change.

2.3. CMIP6 Data and Ensemble Method. Projected precipitation change is needed to generate the reservoir rule curve for the future. Here, we firstly describe the future scenario selection and then introduce the method to calculate weighted mean precipitation from multiple model outputs. CMIP aims to better understand climate changes in a multimodel context. The model performance is assessed by a set of experiments with idealized and historical radiative forcings. Future climate change simulations are based on designed scenarios [36]. CMIP has developed in phases with expanded number and complexity of climate models. In CMIP5, four Representative Concentration Pathway (RCP) scenarios (RCP2.6, RCP4.5, RCP6, and RCP8.5) represent different assumptions about atmospheric greenhouse gas concentrations based on population, economic growth, energy, and land use over the twentieth century has been developed [37]. They are labeled after a possible radiative forcing anomaly value (relative to the preindustrial level) in the year 2100. The latest CMIP6 has a new set of paths so-called SSP (shared socioeconomic pathways) scenarios, indicating different future socio-economic projections and political environments [38]. There are five high-priority SSP scenarios defined in terms of challenges to adaptation and mitigation, from an increasingly sustainable world (SSP1) to a high fossil fuel dependent world (SSP5). Combining the five SSP pathways with the different radiative forcings yields

Table 2: Summary of the regression models to predict water inflow by precipitation (P) and evaporation (E).

Model no.	1	2	3	4
Predictors	P	P, P^2	P, E	P, P^2, E
Equation	105.60 P	44.52 P + 0.1829 P^2	131.37 P − 46.00 E	43.11 P + 1.35 E + 0.1849 P^2
R-square (adjusted)	79.30%	86.66%	81.94%	86.63%
R-square (predicted)	78.75%	85.99%	81.35%	85.90%

a scenario matrix and four of them are selected as standard scenarios (SSP585, SSP370, SSP245, and SSP126). It is worth noting that SSP585, SSP245, and SSP126 can be understood as an update or remake of the RCP8.5, RCP4.5, and RCP2.6, while SSP370 is a newly introduced scenario closing the gap between RCP6.0 and RCP8.5. Specifically, SSP370 represents a regional rivalry world that degrades the international priority for addressing environmental concerns and the corresponding forcing by 2100 is 3.7 W/m^2 [38]. On a global scale, the mean Earth surface temperature will increase 3.6°C over 2081–2100 in SSP370 compared to 1850–1900 and this scenario represents the upper limit of plausible future [4]. Therefore, hydroclimate change under the SSP370 pathway in the Meishan reservoir and potential operation change are investigated in this study. A total of 34 models containing precipitation simulation for SSP370 are used and their information is summarized in Table 3 [39]. All CMIP6 model data are downloaded from the Climate Explorer developed by the Royal Netherlands Meteorological Institute [40], including the SSP370 experiment from 2015 to 2100 and the historical run (forced with changing conditions that are consistent with observations) from 1850 to 2014, the latter is used to evaluate the model performance in our study area by comparing with instrumental data.

It is fundamentally impossible to describe all true climate processes in a single model and the uncertainties introduced by choices in the model design cannot be addressed by varying its parametrizations. Multimodel ensemble strategy is a way to exploit the advantage and to avoid the weakness of individual models due to substantial reduction of the systematic errors in individual models, and multimodel means often agree better with observations than individual model results [20]. In this study, we compute the multimodel mean by both equally and unequally weighted methods and select the best one to predict future precipitation. Note that some of the models have multiple ensemble members with different initial conditions. Therefore, there are three equally weighted multimodel ensemble methods: (1) calculating the mean of all members; (2) calculating the mean of all models with only one member per model; (3) first calculating the means of individual models by corresponding members and then calculating the mean of all models. Moreover, the unequal weights are determined through the best subset regression constrained by maximizing adjusted R-square. All model outputs are resized to 192 × 144 horizontal resolution to calculate the ensemble mean.

2.4. Reservoir Rule Curve Calculation. The reservoir rule curve guides the releasing schedule to impound excess water in wet periods and ensure water demand in dry periods because the water demand change is not consistent with the inflow change. Thus, except for water inflow data described in Section 2.2, water demand data are also required to calculate the rule curve. Meishan reservoir project is the main water source of the Shi River irrigation area. The irrigation release flow is 190 m^3/s and the average agricultural water consumption is 10.63×10^8 m^3 per year under the designed assurance level of 80%. In addition, the annual urban water demand is 400×10^4 m^3 and the downstream ecosystem flow is 5.47 m^3/s [28]. The total annual water consumption of the aforementioned water-using sectors is 12.36×10^8 m^3. According to the long-term statistics, the month-by-month water demands of the reservoir are shown in Figure 3(a).

To calculate the rule curve, the first step is identifying the regulation cycle. A complete operation cycle ranges from one day to multiple years, determined by the coefficient of reservoir storage capacity β (proportion of regulating storage to multiyear average inflow). The range of β for daily, seasonally, yearly, and multiyear (or carryover) reservoirs is $\beta \leq 2\%$, $2\% \beta \leq 8\%$, $8\% \beta \leq 20\%$, and $\beta > 20\%$, respectively [41]. In this study, β is equal to 68% (9.57×10^8 m^3/14.05×10^8 m^3, Table 1) such that the reservoir needs to be carryover regulated. Generally, the horizontal axis of the operating rule curve represents time (month or 10-day period unit), and the vertical axis indicates the reservoir water level or storage capacity. There are three time-varying curves between normal pool level and dead water level. The first is the flood limited curve, which constrains the reservoir water level in the flood season. The other two are the lower water supply curve (or upper rule curve) and limited water supply curve (or lower rule curve), guiding the water refill and release strategies. We select 3–6 representative hydrological years, in which the water inflow is close to the water demand, to calculate operating rule curves, as well as associated annual and carryover storage, and the step-by-step computation follows the engineering standard guidance from reference [42]. The elevation-volume relationship [43] is plotted in Figure 3(b).

3. Results

Generally, the regulating year is different from the calendar year, and the former usually starts from the beginning of the flood season and lasts for 12 months. Under the predefined operation schedule of Meishan reservoir, the regulating year is from June to May [43]. However, the reservoir was commissioned more than 60 years ago and the catchment area experienced significant climate change since then. In this section, we first explore how the optimal regulating rules change in the past decades (1969–2008, historical period). Then, we present the future

Table 3: List of CMIP6 models used in this study.

#	Model name	Institution (country)	Resolution (lon × lat)
1	ACCESS-CM2	Commonwealth Scientific and Industrial Research Organisation/ Australian Research Council Centre of Excellence for Climate System Science (Australia)	192 × 144
2	ACCESS-ESM1-5	Commonwealth Scientific and Industrial Research Organisation (Australia)	192 × 145
3	AWI-CM-1-1-MR	Alfred Wegener Institute, Helmholtz Centre for Polar and Marine Research (Germany)	384 × 192
4	BCC-CSM2-MR	Beijing Climate Centre (China)	320 × 160
5	CAMS-CSM1-0	Chinese Academy of Meteorological Sciences (China)	320 × 160
6	CanESM5-CanOE-p2 CanESM5-p2 CanESM5	Canadian Centre for Climate Modelling and Analysis, Environment and Climate Change Canada (Canada)	128 × 64
7	CESM2-WACCM CESM2	National Centre for Atmospheric Research, Climate and Global Dynamics Laboratory (USA)	288 × 192
8	CMCC-CM2-SR5	Fondazione Centro Euro-Mediterraneo sui Cambiamenti Climatici (Italy)	288 × 192
9	CNRM-CM6-1-HR-f2	Centre National de Recherches Meteorologiques/Centre Europeen de Recherche et de Formation Avancee en Calcul Scientifique (France)	720 × 360
10	CNRM-CM6-1-f2		256 × 128
11	CNRM-ESM2-1-f2		
12	EC-Earth3-veg	EC-Earth-Consortium[1]	512 × 256
13	EC-Earth3		
14	FGOALS-f3-L	Chinese Academy of Sciences (China)	360 × 180
15	FGOALS-g3		180 × 80
16	GFDL-ESM4	National Oceanic and Atmospheric Administration, Geophysical Fluid Dynamics Laboratory (USA)	360 × 180
17	GISS-E2-1-G-f2	Goddard Institute for Space Studies (USA)	144 × 90
18	GISS-E2-1-G-p3		
19	INM-CM4-8	Institute for Numerical Mathematics, Russian Academy of Science (Russia)	180 × 120
20	INM-CM5-0		
21	IPSL-CM6A-LR	Institut Pierre Simon Laplace (France)	144 × 143
22	KACE-1-0-G	National Institute of Meteorological Sciences/Korea Meteorological Administration, Climate Research Division (Korea)	192 × 144
23	MIROC-ES2L-f2	Japan Agency for Marine-Earth Science and Technology/ Atmosphere and Ocean Research Institute, the University of Tokyo/National Institute for Environmental Studies/RIKEN Centre for Computational Science (Japan)	128 × 64
24	MIROC6		256 × 128
25	MPI-ESM1-2-HR	Max Planck Institute for Meteorology/Deutscher Wetterdienst/ Deutsches Klimarechenzentrum (Germany)	384 × 192
26	MPI-ESM1-2-LR	Max Planck Institute for Meteorology/Alfred Wegener Institute, Helmholtz Centre for Polar and Marine Research/Deutscher Wetterdienst/Deutsches Klimarechenzentrum (Germany)	192 × 96
27	MRI-ESM2-0-i2	Meteorological Research Institute (Japan)	320 × 160
28	MRI-ESM2-0		
29	NorESM2-LM	NorESM Climate Modeling Consortium[2]	144 × 96
30	NorESM2-MM		288 × 192
31	UKESM1-0-LL-f2	Met Office Hadley Centre/Natural Environment Research Council (UK)/National Institute of Meteorological Sciences/Korea Meteorological Administration, Climate Research Division (Korea)/National Institute of Water and Atmospheric Research (New Zealand)	192 × 144

[1,2] The full consortium list is available at https://github.com/WCRP-CMIP/CMIP6_CVs/blob/master/CMIP6_institution_id.json.

precipitation projection over 2061–2100 in the SSP370 scenario and associated rule curve change.

3.1. Reservoir Rule Curve of the Historical Time. The annual cycle of water inflow and demand is shown in Figure 3(a), and the flood season is from May to September. The irrigation water demand peak (in June) is a little earlier than the water inflow peak (in July) during 1969–2008; consequently, the predefined operation schedule (June to May) frequently suffers from water deficit in the early months. Moreover, the water demand cycle is largely overlapped with the water inflow cycle such that it is difficult to identify the appropriate regulating cycle. Therefore, we plot all possible

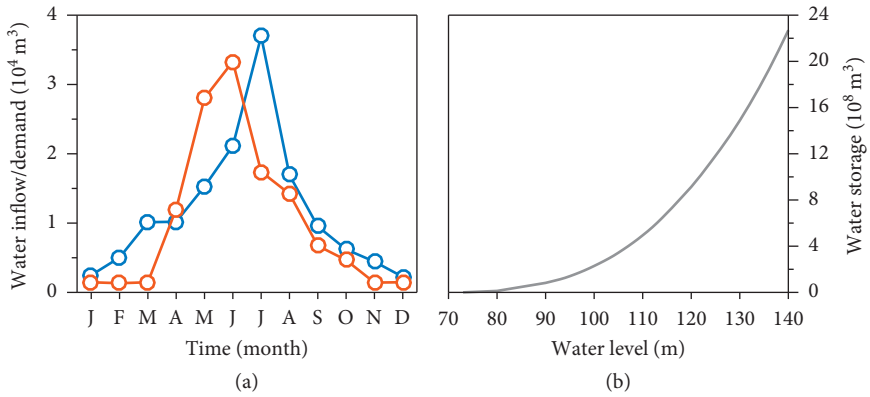

Figure 3: (a) Monthly water inflow (blue) and demand (orange) and (b) the elevation-volume curve.

cases together to make a comparison (Figure 4). For each case, six representative hydrological years (Table 4) are selected to calculate rule curves. Although the total inflow water amount is adjusted to match the water demand, there exist years that the water supply is damaged (negative storage anomaly) due to the uneven seasonal distribution of water inflow. In these cases, the carryover storage needs to be used although it is not a dry year. Therefore, the percentage of damage years is used to screen the appropriate regulating year cycle. On this basis, the best choice is from September to August, which only has one damage year (16.7%). The second optional choice is from July to June (two months later than the beginning of the flood season), which has three damage years (50%). The remaining annual cycles have at least four damage years (>66.7%) while all years are damaged from April to March and May to April. Figure 5 shows the reservoir rule curves starting from July and September, respectively. However, the limiting level during the non-flooded season is 126.0 m, which is lower than the operating water level for seven and five months in the above two cases. Such issues, to some extent, limit the ability of reservoir regulation and utilization of water resources.

3.2. Local Precipitation Change in SSP370 Scenario. Firstly, we evaluate the ability of a set of CMIP6 models to capture the observed changes by Taylor diagram [44] (Figure 6). For a good simulation, the correlation coefficient with the observation and the ratio of their variance should be close to one, while the centered root mean square error (RMSE) should be close to zero. In this study, we test the performance of multiple models in only one grid; thus, the statistics are calculated based on the historical time series instead of the average spatial pattern used in other studies. The statistics for the majority of models are clustered in the intervals in which the correlation coefficients are between 0.35 and 0.55, the ratios of variance are between 45% and 90%, and the centered RMSEs are between 0.8 and 1. The result indicates that most models have a reasonable performance in simulating temporal change of precipitation in the study site, while none of them shows outstanding skills. The three equally weighted multimodel ensemble means also give results that are similar to the best individual model. Moreover, we build the best subset regression ensemble by seven CMIP6 models whose correlation coefficients are larger than 0.5 and it finally maintains five input variables. The regression equation is as follows:

$$Y = 0.13X_2 + 0.17X_{10} + 0.21X_{15} + 0.31X_{22} + 0.13X_{23} + 0.13X_{24} + 0.15X_{26} - 13.64, \quad (1)$$

where Y is the ensemble predicted precipitation, X is the model simulated precipitation, and the subscript number represents the model in Table 3. This unequally weighted multimodel ensemble has the adjusted R-square of 0.43 (equal to the correlation coefficient of 0.66), which has 11% more explained variance than the best individual model (IPSL-CM6A-LR, correlation coefficient = 0.57, RMSE = 0.82) and three equally weighted ensemble methods. Based on the best subset regression, the future precipitation is projected to 2100 (Figure 7). Like the temperature, the annual total rainfall also has a remarkable increasing trend. The precipitation amount of the wettest year reaches 2760 mm in the 2090s, while it is only 831 mm in the driest year in the mid-twenty-first century, indicating that the annual precipitation variability exceeds the envelope range during the past 50-year period (Figure 7(a)). The mean annual precipitation is 2022 mm over 2061–2100, which is 500 mm more than that of 1961–2010. The increased precipitation amount mainly occurs in spring (March to May), while July to September experiences a reduction (Figure 7(b)).

3.3. Reservoir Rule Curve of the 2061–2100 Period. Since the monthly distribution of rainfall changes in the future, the reservoir regulating strategy also needs to be adjusted. We assume that the water demand is the same as the current time and plot all possible regulating cycles for 2061–2100 in Figure 8. It is worth noting that the standard deviation of the weighted ensemble mean is reduced by a factor of $\sqrt{1/N}$ since the ensemble members are sequentially independent and possess an identical standard deviation. Therefore, the range of representative hydrological years of the multimodel ensemble is also reduced. To eliminate this effect, we pick out three representative hydrological years for seven selected

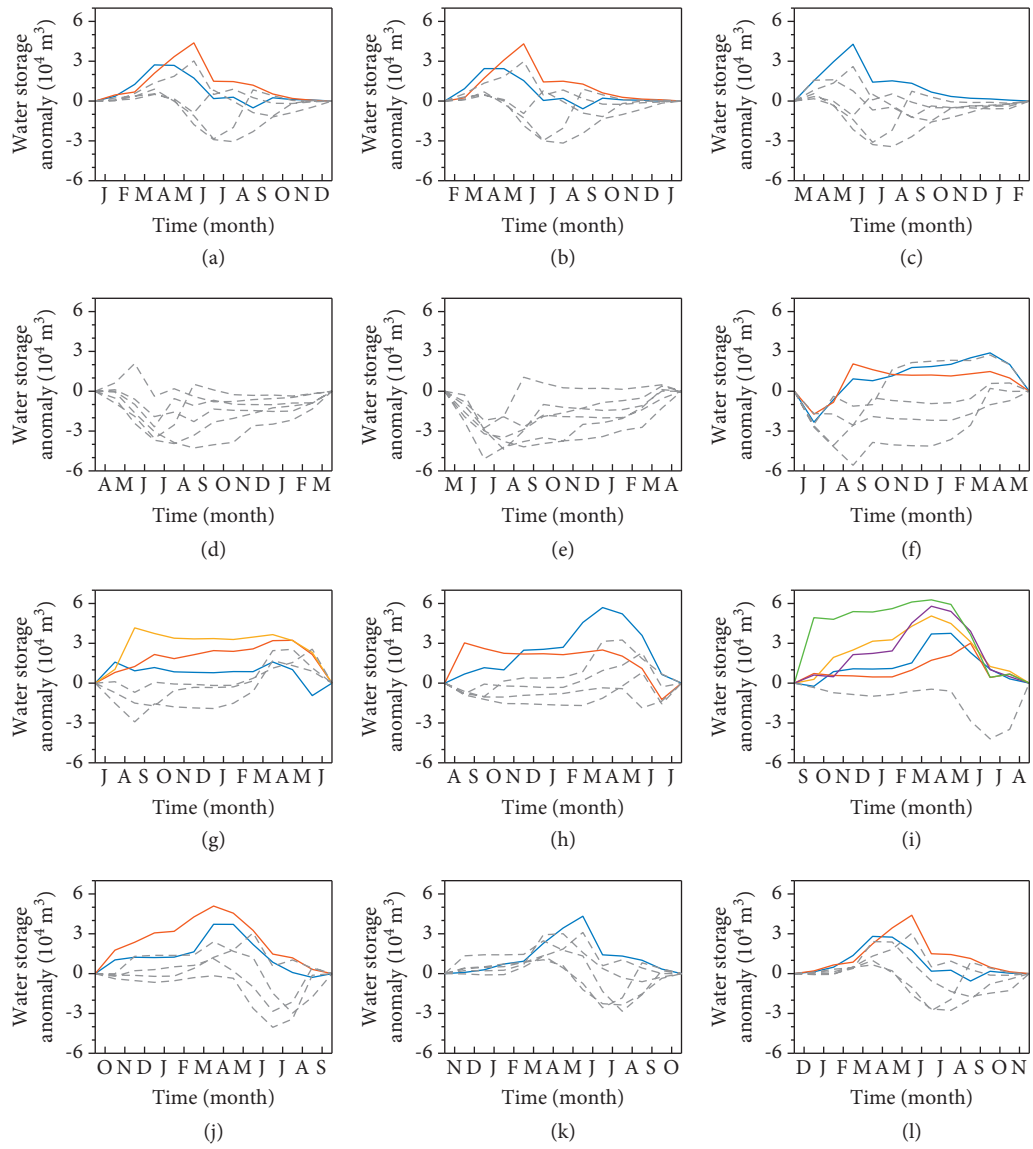

Figure 4: Water storage anomaly for different 12-month regulating cycles in historical time (1969–2008). The curves for damage years (negative storage anomaly for more than two months) are shown by gray dash lines while undamaged years by color solid lines (colors are only used to distinguish multiple lines). (a–l) Regulating cycles start from January to December.

Table 4: Six representative hydrological years under different regulation cycles.

Regulation cycle	Jan-Dec	Feb-Jan	Mar-Feb	Apr-Mar	May-Apr	Jun-May	Jul-Jun	Aug-Jul	Sep-Aug	Oct-Sep	Nov-Oct
Representative hydrological years	1971	1971	1971	1972	1972	1973	1971	1971	1971*	1971*	1971
	1973*	1973*	1973	1973	1973	1977*	1973	1973	1973*	1973	1973
	1974	1974	1974	1974	1984	1985	1979*	1974	1975*	1975*	1983
	1984	1984	1984	1979	1988	1988	1992	1976	1989*	1987	1987
	1998*	1998*	1998*	1984	1997	1992	1993*	1989*	2005*	2003	1997*
	2004	2004	2004	2004	2004	2004*	2004*	2004*	2007	2007	2003

*Undamaged water supply years.

models (Table 5) to generate the rule curves (Figure 8). Similar to the historical period, the number of damage years is least (48%) from September to August. The second optimal cycle is from July to June and November to October, which both have 70% damage years. The cycles with 100% damage years are increased from two to four. The selected rule curves are provided in Figure 9. Compared with the historical period, the annual storage is increased for the July-June scheme while decreased for the September-August scheme. Due to the redistribution of annual precipitation,

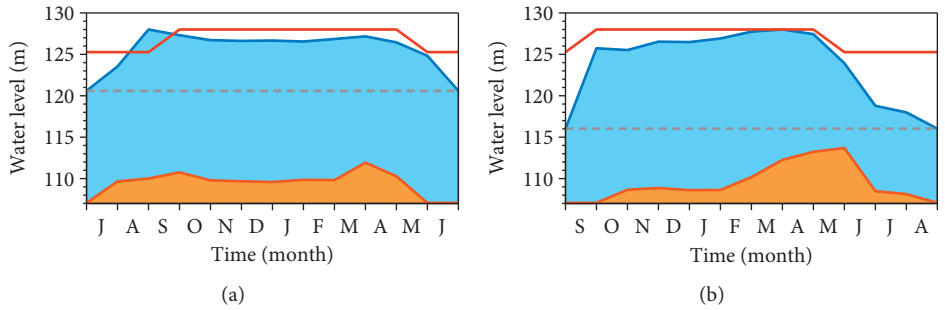

Figure 5: Reservoir rule curves for the July-June scheme (a) and September-August scheme in historical time (1969–2008). The red line is the flood limited curve. The blue/orange line is the lower/limited water supply curve. The gray dash line indicates the threshold of annual and carryover storage.

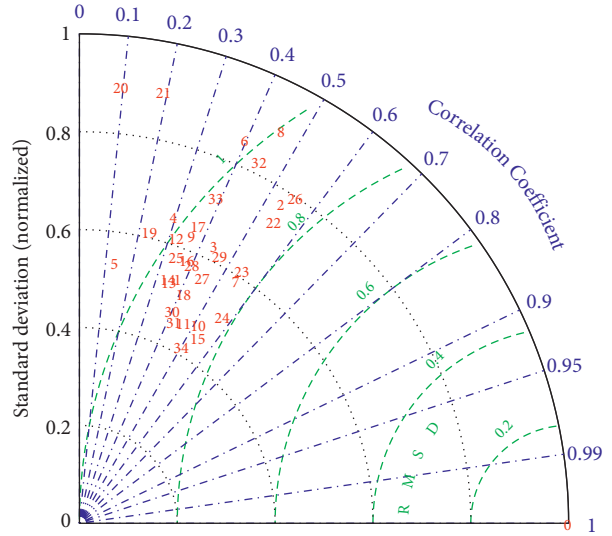

Figure 6: Taylor diagram for precipitation of 34 CMIP6 models. Historical model simulations and observations from 1961 to 2014 are used to calculate the statistics. The number 0 represents observation and models are indicated from 1 to 34 as that in Table 3.

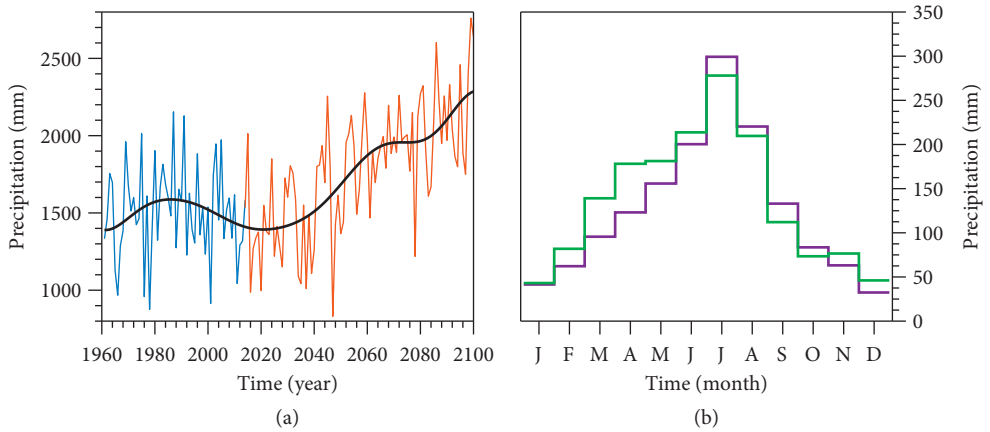

Figure 7: Precipitation change in the Meishan reservoir area in SSP370 scenario. (a) Multimodel ensemble precipitation projection from 2015 to 2100 (orange) and the comparison with the historical observation from 1961 to 2014 (blue). The black line is the 30-year low-pass curve by the Lanczos filter. (b) The monthly precipitation climatology from 1961 to 2014 historical observation (purple) and 2061–2100 multimodel ensemble (green).

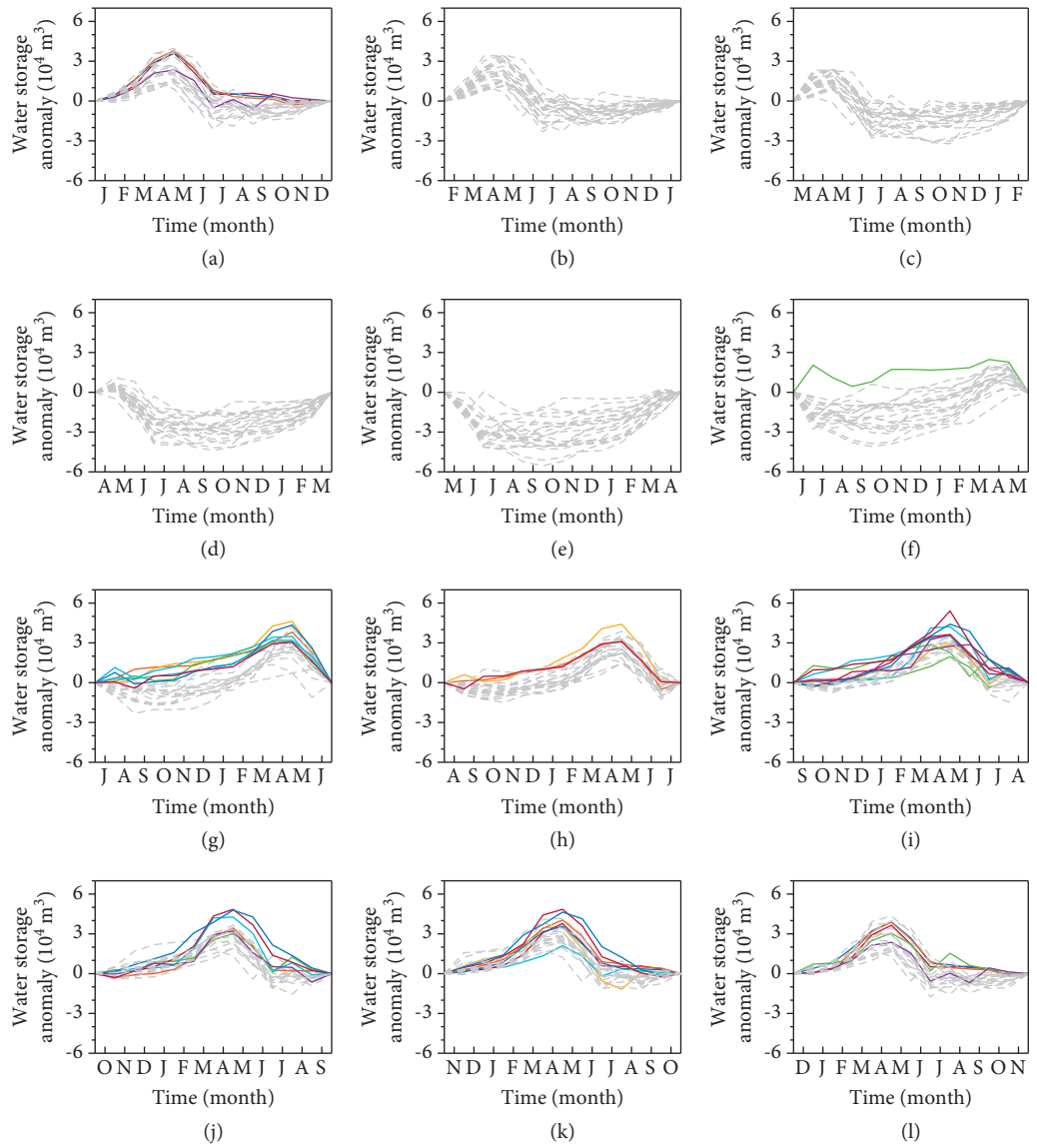

Figure 8: Water storage anomaly for different 12-month regulating cycles in the SSP370 scenario from 2061 to 2100. The curves for damage years (negative storage anomaly for more than two months) are shown by gray dash lines while undamaged years by color solid lines (colors are only used to distinguish multiple lines). (a–l) Regulating cycles start from January to December.

Table 5: Three representative hydrological years under different regulation cycles for five models.

Regulation cycle	Jan-Dec	Feb-Jan	Mar-Feb	Apr-Mar	May-Apr	Jun-May	Jul-Jun	Aug-Jul	Sep-Aug	Oct-Sep	Nov-Oct
ACCESS-ESM1-5	2063	2063	2063	2087	2083	2083	2082	2071*	2062	2062	2062
	2080	2080	2080	2089	2089	2087	2083*	2082	2079	2079	2079*
	2083	2083	2089	2094	2094	2094	2094*	2092*	2082	2082	2082
CESM2	2073	2073	2073	2073	2073	2086	2086*	2072	2072*	2072	2072*
	2086	2086	2086	2086	2090	2089	2090*	2089	2085	2078	2078
	2090	2090	2090	2090	2093	2090	2093	2090	2090*	2089	2089
EC-Earth3-veg	2078*	2066	2066	2066	2077	2084	2066	2077	2065	2065	2077*
	2088*	2078	2078	2077	2094	2087	2087	2087	2077	2077*	2079*
	2096*	2088	2088	2096	2096	2094	2096	2096	2087	2087	2087*
INM-CM4-8	2087	2087	2066	2066	2087	2066	2066	2067	2067*	2067*	2066
	2089	2089	2087	2087	2089	2076	2078	2086	2078*	2086	2086
	2092	2092	2092	2089	2091	2087*	2086	2091	2086*	2091	2091

Table 5: Continued.

Regulation cycle	Jan-Dec	Feb-Jan	Mar-Feb	Apr-Mar	May-Apr	Jun-May	Jul-Jun	Aug-Jul	Sep-Aug	Oct-Sep	Nov-Oct
INM-CM5-0	2068	2068	2068	2068	2068	2068	2068*	2067	2067*	2067*	2067
	2096	2096	2096	2096	2080	2087	2087	2095	2080*	2095*	2095*
	2097	2097	2097	2097	2096	2096	2096	2096	2096*	2096*	2096*
IPSL-CM6A-LR	2069	2071	2069	2066	2069	2069	2068	2074	2068	2068	2074
	2075*	2075	2075	2069	2074	2074	2074	2087	2074	2074	2084
	2096	2096	2096	2074	2085	2083	2095	2095	2095*	2095*	2095
MIROC-ES2L-f2	2077	2079	2079	2079	2079	2079	2076	2094*	2094*	2091	2076
	2098	2095	2092	2094	2092	2094	2087*	2097	2097	2097	2097
	2100	2098	2098	2098	2094	2095	2094*	2099	2099	2099	2099

*Undamaged water supply years.

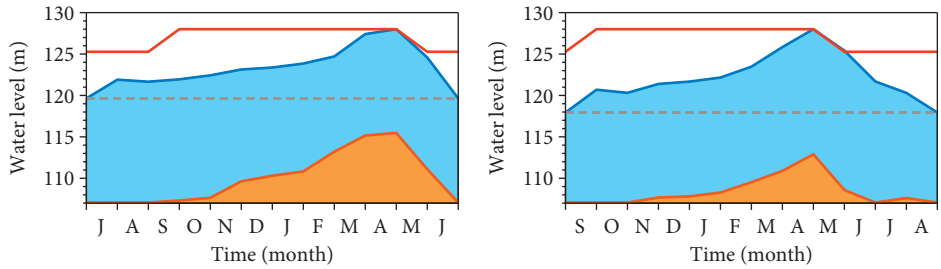

Figure 9: Reservoir rule curves for the July-June scheme (a) and September-August scheme in SSP370 scenario from 2061 to 2100. The red line is the flood limited curve. The blue/orange line is the lower/limited water supply curve. The gray dash line indicates the threshold of annual and carryover storage.

the operating water level is reduced during the nonflooded season and it is lower than the flood control level, indicating that the water supply is no longer affected by flood control in the future. As a result, the efficiency of water utilization is enhanced.

4. Discussion and Conclusions

In this study, we evaluate the impacts of hydroclimate change on the regulating rule curves of the Meishan reservoir constructed in the 1950s, for the historical period (1969–2008) by instrumental data and future period (2061–2100) by CMIP6 simulations. We find that the optimal regulation cycle is from September to August and from July to June for both historical and future periods. The limiting level during the nonflooded season is lower than the operating water level for more than five months in the historical period, which limits the ability of reservoir regulation and utilization of water resources. However, the water supply is no longer affected by flood control in 2061–2100 because of the redistribution of annual precipitation.

Therefore, the predefined operating strategy from June to May is not an efficient scheme for either historical or future scenarios. Operation log of the Meishan reservoir records that the water level is lower than the dead water level in nearly 25% of months from 1965 to 2015, and sometimes even lower than the elevation of irrigation water intake of 95.27 m [27]. Because the operation dead water level is lower than design, the utilization rate of water resources is reduced and the conflicts among water demand sectors are inevitable within the hydrological year. In addition, the associated facilities, such as dam, dike, gate, and plant, will deteriorate more quickly under an abnormal operating condition.

Many large reservoirs in China are designed to provide residential water to metropolises. The population in these cities will continue to grow under the urbanization process in future China [45]. Therefore, the water supply requirement of the large reservoirs is expected to increase year by year. On the contrary, the Meishan reservoir affords water supply for some small counties, which experience a net outflow of population. For example, the population statistics for Jinzhai County, which is the first residential area downstream of the Meishan reservoir, has dropped by 3.49% while the proportion of people aged 65 or above has increased by 6.33% from 2010 to 2020 [46]. Therefore, the demand for urban water is not expected to increase. Furthermore, the irrigation water demand in the future is likely to stay the same as the current level because the cultivated land area in Anhui Province is stable [47]. Without additional water pressure, the improvement of the total economic benefit of the Meishan reservoir will mainly depend on the increase in the benefit of power generation, which will also help China to reach the carbon peak and neutrality targets. Studies have shown that precipitation in many regions of China will increase under global warming scenarios [48]. The case of Meishan reservoir provides a possible reference for the planning and operation of medium-size

reservoirs in these regions. This study also presents a framework to calculate rule curves from multisource datasets (i.e., geographic raster, construction planning document, and climate data) by using a set of software packages. Rule curves for other similar reservoirs could be calculated following this framework, and the individual dataset or software could be substituted by state-of-the-art products.

Data Availability

The shaded relief map in Figures 1(a) and 1(b) is from GEBCO https://download.gebco.net/. The land cover data for 2015 in Figure 1(c) is from http://maps.elie.ucl.ac.be/CCI/viewer/download.php. The grid monthly precipitation data for China are from http://poles.tpdc.ac.cn/zh-hans/data/653191c3-df99-479b-95bd-a18bee30f2bd/. Requests for access to the inflow data of Meishan reservoir should be made to the corresponding author.

Conflicts of Interest

The authors declare that they have no conflicts of interest.

Acknowledgments

The authors acknowledge World Climate Research Programme's Working Group on Coupled Modelling for coordinating and promoting the CMIP6. The authors thank the climate modeling groups for producing and making available their model output, the Earth System Grid Federation (ESGF) for archiving the data and providing access, and the multiple funding agencies for supporting CMIP6 and ESGF. This work was supported by the Strategic Priority Research Program of the Chinese Academy of Sciences (grant no. XDA23100401) and the National Key Research and Development Program of China (grant no. 2017YFA0605303).

References

[1] F.-J. Chang, L. Chen, and L.-C. Chang, "Optimizing the reservoir operating rule curves by genetic algorithms," *Hydrological Processes*, vol. 19, no. 11, pp. 2277–2289, 2005.

[2] W. H. Wan, J. S. Zhao, and J. B. Wang, "Revisiting water supply rule curves with hedging theory for climate change adaptation," *Sustainability*, vol. 11, no. 7, 2019.

[3] E. Quaranta, G. Aggidis, and R. M. Boes, *Assessing the energy potential of modernizing the European hydropower fleet*, vol. 246, Energy Conversion and Management, Amsterderm, Netherlands, 2021.

[4] IPCC, *Climate Change 2021: The Physical Science Basis. Contribution of Working Group I to the Sixth Assessment Report of the Intergovernmental Panel on Climate Change,* Cambridge University Press, Cambridge, England, 2021.

[5] S. Yan, J. Y. Liu, X. H. Gu, and D. D. Kong, "Global runoff signatures changes and their response to atmospheric environment, GRACE water storage, and dams," *Remote Sensing*, vol. 13, p. 20, 2021.

[6] N. Fayaz, L. E. Condon, and D. G. Chandler, "Evaluating the sensitivity of projected reservoir reliability to the choice of climate projection: a case study of bull run watershed, portland, Oregon," *Water Resources Management*, vol. 34, no. 6, pp. 1991–2009, 2020.

[7] H.-I. Eum, A. Vasan, and S. P. Simonovic, "Integrated reservoir management system for flood risk assessment under climate change," *Water Resources Management*, vol. 26, no. 13, pp. 3785–3802, 2012.

[8] D. Raje and P. P. Mujumdar, "Reservoir performance under uncertainty in hydrologic impacts of climate change," *Advances in Water Resources*, vol. 33, no. 3, pp. 312–326, 2010.

[9] A. Kangrang, H. Prasanchum, and R. Hormwichian, "Development of future rule curves for multipurpose reservoir operation using conditional genetic and tabu search algorithms," *Advances in Civil Engineering*, vol. 2018, 2018.

[10] T. Thongwan, A. Kangrang, and H. Prasanchum, "Multi-objective future rule curves using conditional tabu search algorithm and conditional genetic algorithm for reservoir operation," *Heliyon*, vol. 5, no. 9, Article ID e02401, 2019.

[11] M. Mulligan, A. van Soesbergen, and L. Sáenz, "GOODD, a global dataset of more than 38,000 georeferenced dams," *Scientific Data*, vol. 7, no. 1, p. 31, 2020.

[12] P. C. Qin, H. M. Xu, and M. Liu, "Assessing concurrent effects of climate change on hydropower supply, electricity demand, and greenhouse gas emissions in the Upper Yangtze River Basin of China," *Applied Energy*, vol. 279, 2020.

[13] W. J. Zhong, J. Guo, and L. Chen, "Future hydropower generation prediction of large-scale reservoirs in the upper Yangtze River basin under climate change," *Journal of Hydrology*, vol. 588, 2020.

[14] Y. Feng, J. J. Xu, and Y. Hong, "Reservoir scheduling using a multi-objective cuckoo search algorithm under climate change in jinsha river, China," *Water*, vol. 13, no. 13, 2021.

[15] Y. Zhou and S. Guo, "Incorporating ecological requirement into multipurpose reservoir operating rule curves for adaptation to climate change," *Journal of Hydrology*, vol. 498, pp. 153–164, 2013.

[16] S. Wu, J. Zhao, X. Lei, Z. Wang, and H. Wang, "Impacts of climate change on operation of Xin'an River reservoir and adaption strategies," *Journal of Hydroelectric Engineering*, vol. 36, pp. 50–58, 2017.

[17] T. Yan, J. Bai, T. Arsenio, J. Liu, and Z. Shen, "Future climate change impacts on streamflow and nitrogen exports based on CMIP5 projection in the Miyun Reservoir Basin, China," *Ecohydrology and Hydrobiology*, vol. 19, no. 2, pp. 266–278, 2019.

[18] Y. Guo, G. Fang, X. Wen, X. Lei, Y. Yuan, and X. Fu, "Hydrological responses and adaptive potential of cascaded reservoirs under climate change in Yuan River Basin," *Hydrology Research*, vol. 50, no. 1, pp. 358–378, 2019.

[19] C. Wu, G. Huang, H. Yu, Z. Chen, and J. Ma, "Impact of climate change on reservoir flood control in the upstream area of the beijiang River basin, south China," *Journal of Hydrometeorology*, vol. 15, no. 6, pp. 2203–2218, 2014.

[20] C. Tebaldi and R. Knutti, "The use of the multi-model ensemble in probabilistic climate projections," *Philosophical Transactions of the Royal Society A: Mathematical, Physical & Engineering Sciences*, vol. 365, no. 1857, pp. 2053–2075, 2007.

[21] E. Zhao, *Dam Safety Monitoring Data Analysis Theory and Assessment Methods*, Hohai University Press, Nanjing, China, 2018, (in Chinese).

[22] S. Wang, H. Xu, W. Yang, and X. Zhang, "Estimated projections in climate change and meteorological drought in Anhui Province under 1.5 and 2°C global warming based on RCP," *Journal of China Agricultural University*, vol. 23, no. 6, pp. 100–107, 2018, (in Chinese).

[23] Y. Yao, W. Qu, and J. X. Lu, "Responses of hydrological processes under different shared socioeconomic pathway scenarios in the huaihe River basin," *China, Water*, vol. 13, no. 8, 2021.

[24] H. I. Reuter, A. Nelson, and A. Jarvis, "An evaluation of void filling interpolation methods for SRTM data," *International Journal of Geographic Information Science*, vol. 21, no. 9, pp. 983–1008.

[25] W. Schwanghart and D. Scherler, "Short Communication: TopoToolbox 2 - MATLAB-based software for topographic analysis and modeling in Earth surface sciences," *Earth Surface Dynamics*, vol. 2, no. 1, pp. 1–7, 2014.

[26] Q. Xu, L. Ren, J. Liu, B. Yang, and X. Liu, "Forecast model of reservoir inflow based on DEM and its system development," *Chinese Journal of Geotechnical Engineering*, vol. 30, no. 11, pp. 1748–1751, 2008.

[27] L. Zhang, L. Wu, and J. Jin, "Study of staged drought-limited water level of the main reservoir in the large-scale irrigation district," *Journal of Hydraulic Engineering*, vol. 49, no. 6, pp. 757–766, 2018.

[28] Z. Liu, "Studies on regulation modes of meishan reservoir," *China Water Resources*, vol. 9, pp. 30-31, 2018.

[29] Z. Yin, "Discussion on water utilization and protection of meishan reservoir," *Jianghuai Water Resources Science and Technology*, vol. 3, pp. 5–25, 2012.

[30] C. Wang, "Analysis of comprehensive operation mode of Meishan Reservoir," *Journal of Anhui Technical College of Water Resources and Hydroelectric Power*, vol. 3, no. 1, pp. 15–17, 2003.

[31] Y. Xue, C. Gao, X. Zhang, Y. Xu, and P. Li, "Response of runoff in huaihe river upstream to change of different climate elements," *Journal of China Hydrology*, vol. 37, pp. 22–28, 2017.

[32] S. Wang, H. Xu, L. Liu, Y. Wang, and A. Song, "Projection of the impacts of global warming of 1.5 ˚C and 2.0 ˚C on runoff in the upper-middle reaches of huaihe River basin," *Journal of Natural Resources*, vol. 33, pp. 1966–1978, 2018.

[33] Y. Zhao, J. Zhu, and Y. Xu, "Establishment and assessment of the grid precipitation datasets in China for recent 50 years," *Journal of the Meteorological Sciences*, vol. 34, pp. 414–420, 2014.

[34] National Meteorological Information Center, *Daily Meteorological Dataset of Basic Meteorological Elements of China*, National Surface Weather Station (V3.0).

[35] Y. Ou, "Based on surface water dynamics research and application of grass slope," *Master's Thesis*, Nanchang University, 2012, (in Chinese).

[36] L. Touze-Peiffer, A. Barberousse, and H. Le Treut, "The Coupled Model Intercomparison Project: history, uses, and structural effects on climate research," *Wiley Interdisciplinary Reviews-Climate Change*, vol. 11, no. 4, 2020.

[37] D. P. van Vuuren, J. Edmonds, and M. Kainuma, "The representative concentration pathways: an overview," *Climatic Change*, vol. 109, no. 1-2, pp. 5–31, 2011.

[38] B. C. O'Neill, E. Kriegler, and K. L. Ebi, "The roads ahead: narratives for shared socioeconomic pathways describing world futures in the 21st century," *Global Environmental Change-Human and Policy Dimensions*, vol. 42, pp. 169–180, 2017.

[39] V. Eyring, S. Bony, G. A. Meehl et al., "Overview of the coupled model Intercomparison project phase 6 (CMIP6) experimental design and organization," *Geoscientific Model Development*, vol. 9, no. 5, pp. 1937–1958, 2016.

[40] Royal Netherlands Meteorological Institute, "Climate explorer".

[41] Y. Shang, S. Lu, Y. Ye et al., "China' energy-water nexus: hydropower generation potential of joint operation of the Three Gorges and Qingjiang cascade reservoirs," *Energy*, vol. 142, pp. 14–32, 2018.

[42] Z. Cui, *Operation Scheduling of Small and Medium Reservoirs*, Hohai University Press, Nanjing, China, 2017, (in Chinese).

[43] A. Ding, "Study on operations optimization of meishan reservoir," Master's Thesis, Hefei University of Technology, 2010.

[44] K. E. Taylor, "Summarizing multiple aspects of model performance in a single diagram," *Journal of Geophysical Research: Atmospheres*, vol. 106, no. D7, pp. 7183–7192, 2001.

[45] Y. Chen, F. Guo, J. Wang, W. Cai, C. Wang, and K. Wang, "Provincial and gridded population projection for China under shared socioeconomic pathways from 2010 to 2100," *Scientific Data*, vol. 7, no. 1, p. 83, 2020.

[46] Jinzhai County People's Government, *Report for Jinzhai County of the Seventh National Population Census*.

[47] S. Hu, L. Chen, L. Li et al., "Simulation of land use change and ecosystem service value dynamics under ecological constraints in Anhui province, China," *International Journal of Environmental Research and Public Health*, vol. 17, no. 12, 2020.

[48] T. Li, Z. H. Jiang, and H. L. Treut, "Machine learning to optimize climate projection over China with multi-model ensemble simulations," *Environmental Research Letters*, vol. 16, no. 9, 2021.